

PAPER

Anomalous reactivity of supported V₂O₅ nanoparticles for propane oxidative dehydrogenation: influence of the vanadium oxide precursor

Cite this: *Dalton Trans.*, 2013, **42**, 12644

Carlos A. Carrero,^a Christopher J. Keturakis,^b Andres Orrego,^{a,c}
Reinhard Schomäcker^a and Israel E. Wachs^{*b}

The oxidative dehydrogenation (ODH) of propane to propylene by supported vanadia catalysts has received much attention in recent years, but different reactivity trends have been reported for this catalytic reaction system. In the present investigation, the origin of these differing trends are investigated with synthesis of supported V/SiO₂, V/TiO₂, and V/Al₂O₃ catalysts prepared with three different vanadium oxide precursors (2-propanol/vanadyl triisopropoxide [VO(O-Pri)₃] (VTI), oxalic acid/ammonium metavanadate [NH₄VO₃] (AMV), and toluene/vanadyl acetylacetonate [VO(C₅H₇O₂)₂] (VAA)) in order to elucidate the influence of the precursor on supported vanadia phase and propane ODH activity. *In situ* Raman spectroscopy revealed that the choice of vanadium precursor does not affect the dispersion of the supported vanadium oxide phase below 4 V nm⁻² (0.5 monolayer coverage), where only isolated and oligomeric surface VO₄ species are present, and only the AMV precursor favors crystalline V₂O₅ nanoparticle (NP) formation below monolayer coverage (8 V nm⁻²). The propane ODH specific reactivity trend demonstrated that there is no significant difference in TOF for the isolated and oligomeric surface VO₄ sites. Surprisingly, V₂O₅ NPs in the ~1–2 nm range exhibit anomalously high propane ODH TOF values for the supported vanadia catalysts. This was found for all supported vanadium oxide catalysts examined. This comparative study with different V-precursors and synthesis methods and oxide supports finally resolves the debate in the catalysis literature about the dependence of TOF on the surface vanadium density that is related to the unusually high reactivity of small V₂O₅ NPs.

Received 5th March 2013,

Accepted 25th April 2013

DOI: 10.1039/c3dt50611h

www.rsc.org/dalton

1. Introduction

Olefins (alkenes) are the fundamental building blocks of the petrochemical and refining industries for manufacturing important commodities such as polymers, synthetic fibers, and fuel components.¹ Specifically, ethylene and propylene are utilized for commodity manufacturing, whereas higher olefins are used in making fuel components. The traditional method of obtaining light olefins is by Fluid Catalytic Cracking (FCC), but dehydrogenation of light alkanes is the most direct and selective way to obtain a desired olefin.¹ Despite some difficulties in developing commercial processes, oxidative dehydrogenation (ODH) of propane is seen as a promising alternative

to meet the current propylene demand, with vanadium-based catalysts shown to have the best yield for ODH.^{2–12}

The nature of supported VO_x phases on oxide supports has received much attention in recent years.^{5,13} Below monolayer coverage on oxide supports (<8 V nm⁻²), the supported VO_x phase is generally present as isolated VO₄ and/or oligomer surface species. Poor dispersion of the VO_x phase on the oxide support, however, may also result in V₂O₅ NPs below monolayer coverage.^{5,13} Above monolayer coverage (>8 V nm⁻²), 3D crystalline V₂O₅ nanoparticles (NPs) are present and NPs grow in dimension with increasing vanadium oxide loading. Raman spectroscopy is the technique of choice for identifying the various supported VO_x phases, especially because it can detect V₂O₅ NPs that are <4 nm in size, a limitation of X-ray Diffraction (XRD).¹⁴ Additionally, UV-vis spectroscopy has been shown to be the technique of choice for quantifying the degree of polymerization of surface VO_x species on oxide supports.¹⁵

There have been conflicting claims in the literature about the relative catalytic contributions of the different supported VO_x structures (isolated VO_x species, oligomeric surface VO_x species and crystalline V₂O₅ NPs) to the catalytic activity of

^aDepartment of Chemistry, Technische Universität Berlin, Straße des 17. Juni 124, D-10623 Berlin, Germany. E-mail: schomaecker@tu-berlin.de; Tel: +49-30-314-24973

^bOperando Molecular Spectroscopy & Catalysis Laboratory, Dept. of Chemical Engineering, Lehigh University, Bethlehem, PA 18015, USA. E-mail: iew0@lehigh.edu; Tel: +1-610-758-4274

^cEnvironmental Catalysis Group, Department of Chemical Engineering, University of Antioquia, Calle 53, # 61-30, Medellín, Colombia

supported vanadia catalysts for propane ODH. Some researchers have reported a significant increase in the catalytic turnover frequency (TOF: reaction rate per VO_x site) with increasing vanadia loading on the support^{8,16–18,20,22,24} while other researchers have found a relatively constant TOF with increasing vanadia loading on the supports.^{19,21,23,25–32} A close examination of the propane ODH catalysis literature reveals several different catalyst synthesis methods have been used by the researchers in this field and it is important to better understand the influence of the different preparation methods on the different supported VO_x structures and their specific TOF values. To address the influence of the synthesis method upon the molecular structure and specific activity of the different supported VO_x phases for propane ODH, a series of supported V/SiO₂, V/TiO₂, and V/Al₂O₃ catalysts were prepared by three different methods and precursors (2-propanol/vanadyl triisopropoxide [$\text{VO}(\text{O-Pri})_3$], oxalic acid/ammonium metavanadate [NH_4VO_3], and toluene/vanadyl acetylacetonate [$\text{VO}(\text{C}_5\text{H}_7\text{O}_2)_2$]).

2. Experimental

2.1 Catalyst preparation

Supported vanadium oxide catalysts were prepared on three different oxide supports, Al₂O₃ (Engelhard, SA = 170 m² g⁻¹), SiO₂ (Cabosil EH-5, SA = 332 m² g⁻¹), and TiO₂ (Degussa P-25, SA = 45 m² g⁻¹). The Al₂O₃ catalysts using a vanadyl acetylacetonate precursor, however, were prepared using a different Al₂O₃ (Alfa Aesar, item no. 43857, SA = 125 m² g⁻¹). The supported AMV catalysts were prepared by the incipient wetness impregnation of ammonium metavanadate (Sigma Aldrich, 99%) + oxalic acid (Alfa Aesar, 10% w/v) solutions, as outlined by Argyle *et al.*³³

The supported VTI catalysts were prepared by the incipient wetness impregnation of vanadyl triisopropoxide (Alfa Aesar, 97% purity) + 2-propanol (Fischer ACS, 99.9% purity) solutions. Oxide support and solution were mixed for 30–45 minutes in a glove box under flowing N₂. After impregnation, the samples were initially dried in the N₂ glove box at room temperature for 24 hours. The samples were transferred to a programmable oven (Thermolyne Model 48000) where they were dried under flowing air (Airgas, zero grade) at 120 °C for 4 hours and finally calcined in flowing air at 500 °C for 3 hours. The ramp rate during calcination was 1 °C min⁻¹.

The supported VAA catalysts were prepared by wet saturation impregnation of a porous γ -alumina (Alfa Aesar, item no. 43857, SA = 125 m² g⁻¹) with a saturated solution of vanadyl acetylacetonate (Sigma Aldrich, >97%) in toluene. Details about the synthesis and characterization can be found elsewhere.^{34,35}

2.2 *In situ* Raman spectroscopy

The Raman spectra of supported vanadium oxide catalysts were obtained with a high resolution, dispersive Raman spectrometer system (Horiba LabRam-HR) equipped with three laser excitations (532, 442, and 325 nm). The lasers were

focused on the samples with a confocal microscope equipped with a 50× long working distance objective (Olympus BX-30-LWD, numerical aperture = 0.50) for the visible wavelengths.

For *in situ* Raman measurements of dehydrated catalysts, 20–50 mg of catalyst powder was placed in an environmentally controlled high temperature reactor (Harrick High-Temperature Reaction Chamber) containing a quartz window. The sample temperature was controlled by a Harrick ATC Temperature Controller unit. To dehydrate the sample, the catalyst was initially heated at a rate of 10 °C min⁻¹ in the *in situ* Harrick cell to 500 °C and held for 30–45 min under 30 mL min⁻¹ flowing 10% O₂/Ar (Airgas 10% O₂/Ar). Spectra were initially collected at 500 °C. Afterward, the sample was allowed to cool, at 10 °C min⁻¹ under an argon atmosphere (30 mL min⁻¹), to room temperature. A second spectrum was collected at room temperature. The Raman spectra were collected using the 532 or 442 nm laser with an accumulation of 3–6 scans at 10–30 seconds per scan and a 200 micron laser hole size. Unless noted, all Raman spectra shown are from room temperature collections using the 532 nm laser.

2.3 *In situ* diffuse reflectance ultraviolet-visible (UV-vis) spectroscopy

The UV-vis spectra of the supported vanadium oxide catalysts were obtained using a Varian Cary 5E UV-vis-NIR spectrophotometer with the Harrick Praying Mantis accessory. Approximately 5–25 mg of each catalyst in finely ground powder form was loaded into an *in situ* environmental cell (Harrick High Temperature Reaction Chamber, HVC-DR2). The catalysts were dehydrated *in situ* at 500 °C using the same dehydration procedure mentioned in §2.2. Spectra of the dehydrated samples were collected in the 200–800 nm range at 300 °C and 200 °C, after the 500 °C dehydration, using a scan rate of 60 nm min⁻¹ and a signal averaging time of 0.2 seconds. A magnesium oxide (MgO) sample was used as a standard for obtaining the background absorbance.

The Kubelka–Munk function $F(R_\infty)$ was calculated from the absorbance of the UV-vis spectra. To minimize the effects of regular reflection and particle size samples were diluted with MgO, up to a 5 : 1-MgO : catalyst ratio, which gave a $F(R_\infty) \leq 1$. The edge energy (E_g), or band gap, was determined by finding the intercept of the straight line for the low-energy rise of a plot of $[F(R_\infty)h\nu]^2$ versus $h\nu$, where $h\nu$ is the incident photon energy.¹⁵

2.4 Steady-state ODH reaction

The steady-state ODH catalytic measurements were performed at ambient pressure with U-shaped fixed bed quartz reactors (i.d. 6 mm). The powder pristine catalysts were pressed and sieved at particles sizes between 200 and 300 μm being suitable particle sizes to discard mass transfer limitations.³⁴ In order to avoid hot spots and homogenize the temperature gradient inside the catalyst bed, the catalyst pellets were diluted with same particle size inert silicon carbide (SiC) in the mass ratio 1 : 2 (catalyst-SiC). The reactor, containing the diluted catalyst between two layers of SiC, was immersed into a

fluidized bed of sand serving as a source of heat to provide 8 cm long isothermal conditions. The reactant feed consisted of synthetic air (20.5% O₂ in N₂) and propane (99.9% C₃H₈). The flow rates were controlled separately by two electronic mass flow controllers calibrated in advance (Bronkhost Hi-Tech, E1-flow mass flow controller). The reactant mixture passed a static mixer prior to entering the reactor. Exhaust gases were analyzed by an on-line gas chromatograph (GC, Shimadzu 2014) equipped with two packed columns (HayeSep Q and molecular sieve 13×) for the separation of O₂, N₂, CO, CO₂, and C1–C3 hydrocarbons. Oxygen and nitrogen were detected by a thermal conductivity detector, whereas hydrocarbons and methanized carbon oxides were detected by a flame ionization detector. The duration of each GC analysis was about 27 minutes, which is long enough to achieve steady state behavior after a change in reaction conditions, which was experimentally determined to take about 10 minutes. Bare support materials were measured showing negligible reactivity under reaction conditions.

Experiments using pure SiC were also carried out demonstrating the absence of homogeneous gas phase reaction below 550 °C. Carbon balance was closed up to 100 ± 5%. Experimental error for the V/SiO₂ and V/TiO₂ catalysts was determined from multiple runs. The average observed error for V/SiO₂ and V/TiO₂ was 4.5%, with a maximum of 14%. The average error is considered the error for the V/Al₂O₃ measurements. Turn-over frequencies (TOFs) were calculated by dividing the propane consumption rate (mol C₃H₈ (kg catalyst s)⁻¹, from GC analysis) by the theoretical vanadium loading (mol V kg catalyst⁻¹).

3. Results

3.1 Supported V/Al₂O₃ catalysts

3.1.1 *In situ* Raman spectroscopy

3.1.1.1 Vanadyl triisopropoxide (VTI) precursor. The *in situ* Raman spectra of the dehydrated supported vanadyl triisopropoxide catalysts are presented in Fig. 1, with V loadings ranging from 0.7–9.5 V nm⁻². All the catalysts exhibit a band at 1020–1034 cm⁻¹ assigned to the vanadyl (V=O) stretch of surface mono-oxo VO₄ species.^{30,33,36–38} The shift from 1020–1035 cm⁻¹ reflects the oligomerization of the surface VO₄ species with surface VO_x coverage.³⁹ Additionally, bands at 145, 198, 287, 308, 413, 491, 535, and 1002 cm⁻¹ are present from crystalline V₂O₅ NPs.⁴⁰ Nanoparticle formation occurs for catalysts with V loadings of 7.7 V nm⁻² or greater, which corresponds to monolayer surface coverage (~8 V nm⁻²).⁴¹ The supported V₂O₅ NP bands at 491 and 535 cm⁻¹ are broad while the typical 705 cm⁻¹ band for crystalline V₂O₅ is absent indicating that these supported V₂O₅ NPs are not large or well ordered. The broad bands at ~500 and ~810 cm⁻¹ observed for the low loading samples arise from the Al₂O₃ support spectrum, as shown in Fig. 1, but most likely originate from the *in situ* reactors quartz window as alumina supports typically do not possess any Raman active modes.^{30,42}

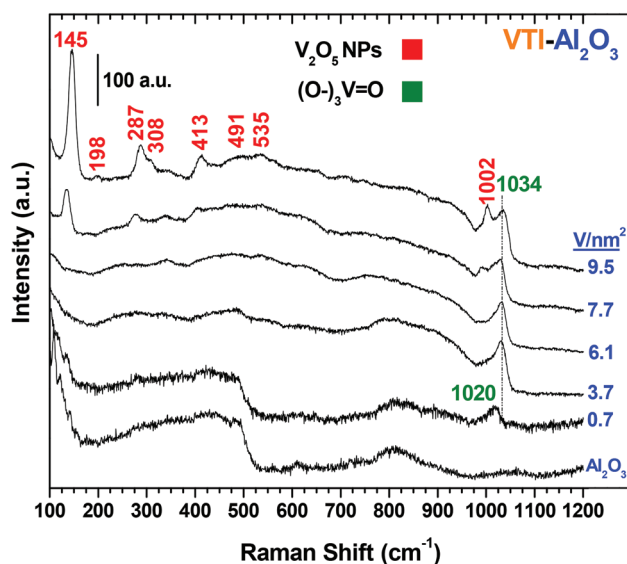


Fig. 1 *In situ* Raman spectroscopy (532 nm) of dehydrated (500 °C) supported V/Al₂O₃ catalysts as a function of surface vanadium density (V atoms per nm²) prepared by impregnation of vanadyl triisopropoxide (VTI) precursor in isopropanol.

3.1.1.2 Vanadyl acetylacetonate (VAA) precursor. The *in situ* Raman spectra of the dehydrated supported vanadyl acetylacetonate catalysts are presented in Fig. 2 with V loadings ranging from 2.1 to 5.3 V nm⁻². Note that a different alumina support was used for these supported V/Al₂O₃ catalysts from the VAA precursor (see Catalyst synthesis section 2.1) and does not give rise to Raman active modes. All the catalysts possess a band at 1006–1025 cm⁻¹ reflecting isolated and partly oligomerized surface mono-oxo VO₄ species, respectively.^{30,33,36–38} A band at 251 cm⁻¹ is visible for the 2.1 V nm⁻² catalyst and is

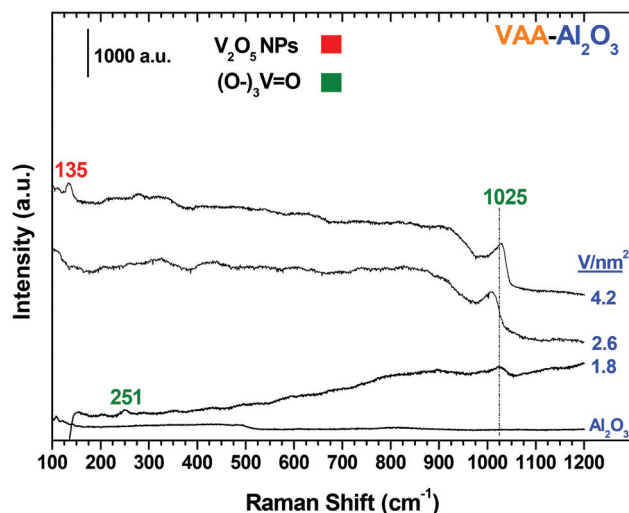


Fig. 2 *In situ* Raman spectroscopy (532 nm) of dehydrated (500 °C) supported V/Al₂O₃ catalysts as a function of surface vanadium density (V atoms per nm²) prepared by impregnation of vanadyl acetylacetonate (VAA) precursor in a toluene solvent. Note: the 1.8 V nm⁻² sample was collected using a 442 nm laser due to strong sample fluorescence.

assigned to the V–O–V bending mode of oligomeric surface VO_4 species.⁴³ This spectrum was collected using the 442 nm excitation wavelength that apparently provides resonance enhancement of this vibrational mode. For the supported 4.2 V nm^{-2} catalyst, a small band at 135 cm^{-1} is observed characteristic of V_2O_5 NPs. This suggests that the VAA precursor can result in a small amount of V_2O_5 NPs below monolayer surface coverage ($\sim 8 \text{ V nm}^{-2}$). The $\sim 10 \text{ cm}^{-1}$ red shift of the V=O frequencies from the VAA precursor compared to the VTI precursor indicates that the surface VO_4 species are slightly less polymerized from the VAA precursor than from the VTI precursor on the alumina support at comparable surface vanadium density.

3.1.1.3 Ammonium metavanadate (AMV) precursor. The *in situ* Raman spectra of the dehydrated (500 °C) ammonium metavanadate catalysts are presented in Fig. 3 with V loadings ranging from 3.7 to 9.5 V nm^{-2} (monolayer $\sim 8 \text{ V nm}^{-2}$). The supported VO_x catalysts with vanadium loadings $< 3.7 \text{ V nm}^{-2}$ exhibited intense fluorescence that prevented collection of their Raman spectra. All the supported AMV catalysts possess a Raman band at 1035 cm^{-1} , assigned to the vanadyl (V=O) stretch of oligomeric surface mono-oxo VO_4 species.^{30,33,36–38} Sharp bands at 140, 194, 283, 302, 404, 482, 528, 705, and 998 cm^{-1} are from crystalline V_2O_5 nanoparticles (NPs). The V_2O_5 NPs give rise to all the Raman bands of well-ordered V_2O_5 crystals indicating that the NPs are slightly larger and more ordered when the AMV precursor is employed than when the VTI precursor is employed. Nanoparticle formation occurs for samples with V loadings of 6.1 V nm^{-2} or greater, indicating that the AMV precursor causes V_2O_5 NP formation even below monolayer coverage ($\sim 8 \text{ V nm}^{-2}$). The broad bands at ~ 500 and $\sim 810 \text{ cm}^{-1}$ observed for the low loading samples arise from the Al_2O_3 support spectrum, as shown in Fig. 1, but

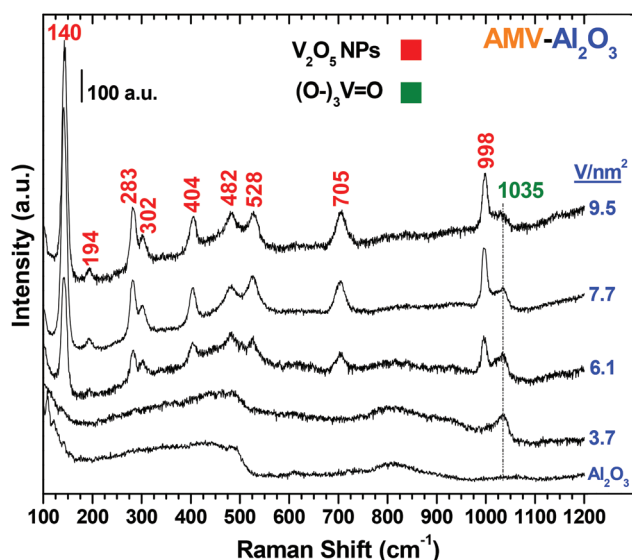


Fig. 3 *In situ* Raman spectroscopy (532 nm) of dehydrated (500 °C) supported $\text{V}/\text{Al}_2\text{O}_3$ catalysts as a function of surface vanadium density (V atoms per nm^2) prepared by impregnation of ammonium metavanadate (AMV) precursor in aqueous oxalic acid.

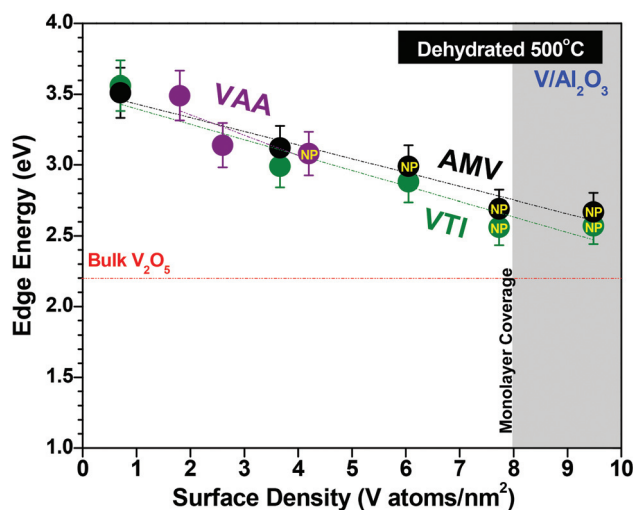


Fig. 4 Vanadia UV-vis edge energy (or optical bandgap, eV) of supported $\text{V}/\text{Al}_2\text{O}_3$ catalysts as a function of surface vanadium density and precursor. Edge energies were obtained from *in situ* UV-vis spectra of the dehydrated (500 °C) catalysts. “NP” indicates that crystalline V_2O_5 nanoparticles were detected by Raman spectroscopy. Precursors: AMV = ammonium metavanadate/aqueous oxalic acid, VTI = vanadyl triisopropoxide/isopropanol, VAA = vanadyl acetylacetonate/toluene.

most likely originate from the *in situ* reactors quartz window as alumina supports typically do not possess any Raman active modes.^{30,42}

3.1.2 In situ UV-vis spectroscopy. The *in situ* UV-vis optical edge energy (E_g) values of the dehydrated supported $\text{VO}_x/\text{Al}_2\text{O}_3$ catalysts, prepared from the VTI, VAA, and AMV precursors, are presented in Fig. 4. The edge energy values range from 2.5 to 3.6 eV, with the highest E_g value indicating that the surface VO_4 species have a high degree of isolation for the supported 0.7 $\text{V}/\text{Al}_2\text{O}_3$ catalysts.¹⁵ The decreasing E_g trend with increasing vanadia loading indicates a higher degree of polymerization (formation of bridging V–O–V bonds of polyvanadates), culminating in the formation of crystalline V_2O_5 NPs at the highest loadings. The extent of polymerization of the surface VO_4 species, as reflected in the decreasing E_g value, for all precursors is very similar within experimental error reflecting the insensitivity of UV-vis E_g values between these three sets of catalysts. This is consistent with the Raman results that the V_2O_5 NPs only constitute a small fraction of the supported VO_x phase.

3.1.3 Steady-state propane ODH reaction. The steady-state turnover-frequency (TOF) for propane oxidative dehydrogenation (ODH) as a function of surface density and precursor used are given in Fig. 5. The reaction conditions correspond to 500 °C with a reactant composition of $\text{C}_3\text{H}_8\text{-O}_2 = 2 : 1$. Catalyst mass (5–20 mg) or total flow rate (20–120 mL min^{-1}) was varied to find suitable residence times for propane conversions below 10% that allows a correct calculation of TOFs at the given feed composition. At the same time O_2 conversion is far from complete. The propane TOF trend for the AMV precursor exhibits a dependence on vanadia loading and is a bell-shaped curve with a maximum TOF occurring around

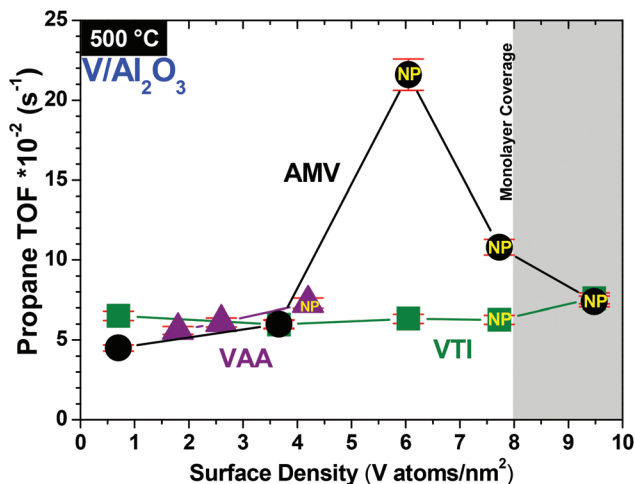


Fig. 5 Steady-state turnover-frequencies (TOFs) for supported V/Al_2O_3 catalysts during propane oxidative dehydrogenation (ODH) as a function of surface vanadium density and precursor. The reaction conditions correspond to 500 °C with a reactant composition of $C_3H_8-O_2 = 2 : 1$. Catalyst mass (5–20 mg) or total flow rate (20–120 mL min^{-1}) was varied to find suitable residence times for propane conversions below 10%. “NP” indicates that crystalline V_2O_5 nanoparticles were detected by Raman spectroscopy. Precursors: AMV = ammonium metavanadate/aqueous oxalic acid, VTI = vanadyl triisopropoxide/isopropanol, VAA = vanadyl acetylacetonate/toluene.

$6.1 V nm^{-2}$, as similarly reported by Argyle *et al.*³³ The TOF value for the VTI precursor is constant until the highest loading at which point it slightly increases from 6.3 to $7.6 \times 10^{-2} s^{-1}$. The VAA precursor gives rise to a slight increase in TOF from 5.6 to $7.3 \times 10^{-2} s^{-1}$. At low surface VO_x coverage, all the catalysts exhibit almost the same propane ODH TOF value that is independent of surface VO_x coverage (0.7 – $4 V nm^{-2}$). These results demonstrate that the use of different vanadium precursors in the preparation of supported VO_x catalysts can indeed result in different reactivity trends for propane ODH, especially at high surface vanadia coverage on alumina ($>4 V nm^{-2}$).

3.2 Supported V/SiO_2 catalysts

3.2.1 *In situ* Raman spectroscopy

3.2.1.1 VTI precursor. The *in situ* Raman spectra of the dehydrated supported vanadyl triisopropoxide catalysts are presented in Fig. 6 with V loadings ranging from 0.4 to $3.4 V nm^{-2}$ (maximum dispersion $\sim 2.6 V nm^{-2}$ for SiO_2).⁴⁴ All the catalysts possess a Raman band at $\sim 1037 cm^{-1}$, assigned to the vanadyl ($V=O$) stretch of isolated surface mono-oxo VO_4 species.^{30,36,40,44} The broad Raman bands at ~ 500 , ~ 604 , and $\sim 810 cm^{-1}$ originate from the SiO_2 support.⁴⁴ Additionally, the SiO_2 support band at $\sim 480 cm^{-1}$ is likely an artifact since it has not been seen in previous Cabosil EH-5 SiO_2 spectra.^{40,44} Several samples exhibit broad bands at ~ 913 and $\sim 1077 cm^{-1}$ which are characteristic of $Si(-O^-)_2$ and $Si-O^-$ functionalities, respectively, that have been perturbed by vanadium oxide deposition^{44,45} and indicate formation of bridging $V-O-Si$ bonds. The catalyst with the $1 V nm^{-2}$ loading possesses a very small band at $\sim 140 cm^{-1}$ from traces of V_2O_5 NPs in this sample. The absence of strong Raman features characteristic

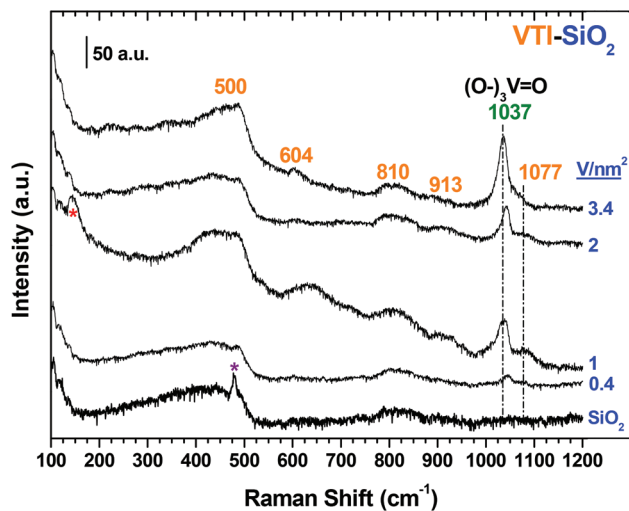


Fig. 6 *In situ* Raman spectroscopy (532 nm) of dehydrated (500 °C) V/SiO_2 catalysts as a function of surface vanadium density (V atoms per nm^2) prepared by impregnation of vanadyl triisopropoxide (VTI) precursor in isopropanol. The “*” for the SiO_2 spectrum indicates a spectral artefact.

of crystalline V_2O_5 NPs indicates that the NPs are essentially not present in the supported V/SiO_2 samples prepared with the VTI precursor.

3.2.1.2 AMV precursor. The *in situ* Raman spectra of the dehydrated (500 °C) supported ammonium metavanadate catalysts are presented in Fig. 7, with V loadings ranging from 0.9 to $3.2 V nm^{-2}$ (maximum dispersion $\sim 2.6 V nm^{-2}$).⁴⁴ All the catalysts possess a band at $\sim 1036 cm^{-1}$, assigned to the vanadyl ($V=O$) stretch of the isolated surface mono-oxo VO_4 species.^{30,36,40,44} Both the supported 0.9 and $1.8 V nm^{-2}$ samples also exhibit a small broad band at $\sim 928 cm^{-1}$ that is characteristic of $Si(-O^-)_2$ functionalities that have been

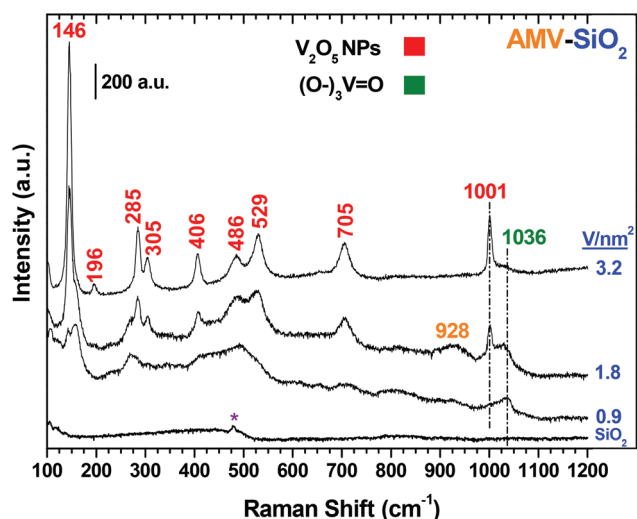


Fig. 7 *In situ* Raman spectroscopy (532 nm) of dehydrated (500 °C) supported V/SiO_2 catalysts as a function of surface vanadium density (V atoms per nm^2) prepared by impregnation of ammonium metavanadate (AMV) precursor in aqueous oxalic acid. The “*” for the SiO_2 spectrum indicates a spectral artefact.

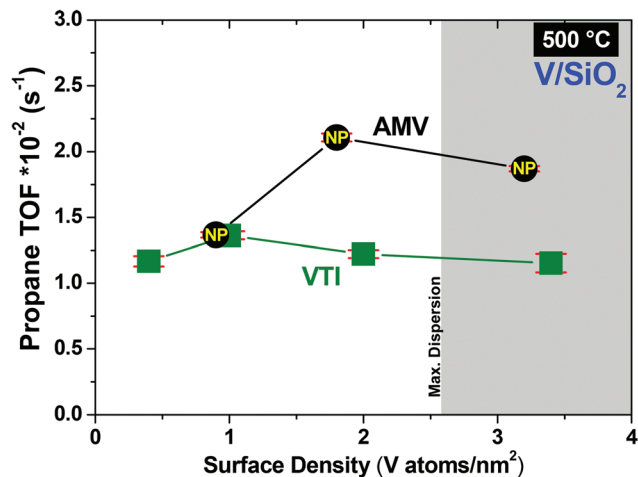


Fig. 8 Steady-state turnover-frequencies (TOFs) for supported V/SiO₂ catalysts during propane oxidative dehydrogenation (ODH) as a function of surface density and precursor. Reaction conditions correspond to 500 °C with a reactant composition of C₃H₈-O₂ = 2 : 1. Catalyst mass (13–50 mg) or total flow rate (100–140 mL min⁻¹) was varied to find suitable residence times for propane conversions around 10%. “NP” indicates that crystalline V₂O₅ nanoparticles were detected by Raman spectroscopy. Precursors: AMV = ammonium metavanadate/aqueous oxalic acid, VTI = vanadium triisopropoxide/isopropanol.

perturbed by vanadium oxide deposition^{44,45} and indicates formation of bridging V–O–Si bonds. The additional sharp Raman bands at 146, 196, 285, 305, 406, 486, 529, 705 and 1001 cm⁻¹ correspond to crystalline V₂O₅ nanoparticles (NPs) that are well-ordered. Nanoparticle formation occurs for all samples, indicating that the AMV precursor results in the formation of well-ordered crystalline V₂O₅ NPs below the maximum dispersion limit of vanadium oxide (~2.6 V nm⁻²).⁴⁴

3.2.2 Steady-state propane ODH reaction. The steady-state turn-over-frequency values for propane ODH as a function of surface density and precursor used are given in Fig. 8. Reaction conditions correspond to 500 °C with a reactant composition of C₃H₈-O₂ = 2 : 1. Catalyst mass (13–50 mg) or total flow rate (100–140 mL min⁻¹) was varied to find suitable residence times for propane conversions around 10%. The propane TOF trend for the AMV precursor is somewhat characteristic of a bell-shaped curve with a maximum TOF occurring around 1.8 V nm⁻² with TOF values only varying from 1.4–2.1 × 10⁻² s⁻¹. The TOF value for the VTI precursor with VO_x loading, however, is constant (1.2–1.4 × 10⁻² s⁻¹). For 1 V nm⁻² supported V/SiO₂ catalysts, the TOF values are indistinguishable for the catalysts synthesized from both precursors. At high surface VO_x coverage, the TOF values are greater for the AMV than the VTI supported V/SiO₂ catalysts.

3.3 V/TiO₂

3.3.1 *In situ* Raman spectroscopy

3.3.1.1 VTI precursor. The *in situ* Raman spectra of the dehydrated (500 °C) supported vanadyl triisopropoxide catalysts are presented in Fig. 9 with V loadings ranging from 3 to 8.8 V nm⁻² (monolayer ~8 V nm⁻²).⁴¹ Only the 800–1200 cm⁻¹

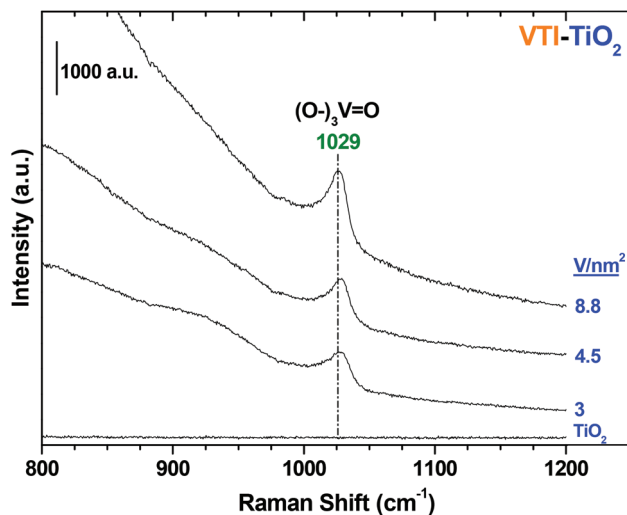


Fig. 9 *In situ* Raman spectroscopy (532 nm) of dehydrated (500 °C) supported V/TiO₂ catalysts as a function of surface vanadium density (V atoms per nm²) prepared by impregnation of vanadium triisopropoxide (VTI) precursor in isopropanol.

region is shown due to intense TiO₂ support vibrations below 800 cm⁻¹.⁴⁶ All the catalysts possess a Raman band at ~1029 cm⁻¹ from the vanadyl (V=O) stretch of surface mono-oxo VO₄ species.^{36,41,46} The absence of strong Raman features characteristic of crystalline V₂O₅ NPs indicates that V₂O₅ NPs are not present in the supported V/TiO₂ samples prepared with the VTI precursor.

3.3.1.2 AMV precursor. The *in situ* Raman spectra of the dehydrated (500 °C) supported ammonium metavanadate catalysts are presented in Fig. 10 with V loadings ranging from 3.0 to 8.8 V nm⁻² (monolayer ~8 V nm⁻²).⁴¹ Only the

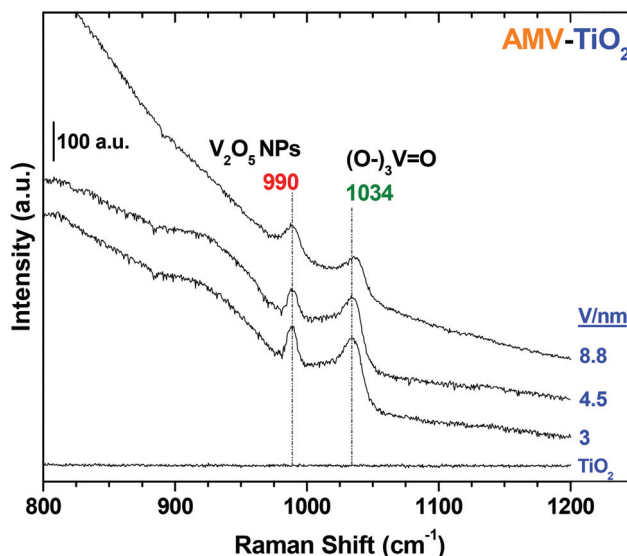


Fig. 10 *In situ* Raman spectroscopy (532 nm) of dehydrated (500 °C) supported V/TiO₂ catalysts as a function of surface vanadium density (V atoms per nm²) prepared by impregnation of ammonium metavanadate (AMV) precursor in aqueous oxalic acid.

800–1200 cm^{-1} region is shown due to intense TiO_2 support vibrations below 800 cm^{-1} .⁴⁶ All the catalysts possess a Raman band at 1034 cm^{-1} , assigned to the vanadyl ($\text{V}=\text{O}$) stretch of surface mono-oxo VO_4 species.^{36,41,46} The additional Raman band at 990 cm^{-1} is characteristic of crystalline V_2O_5 NPs. Nanoparticle formation occurs for all samples, indicating that the AMV precursor results in the formation of crystalline V_2O_5 NPs below monolayer coverage ($\sim 8 \text{ V nm}^{-2}$). The slightly higher vibration of the vanadyl $\text{V}=\text{O}$ bond at 1034 cm^{-1} for the supported V/TiO_2 -AMV catalyst relative to the supported V/TiO_2 -VTI catalysts at 1029 cm^{-1} suggests that the surface vanadia species are somewhat more polymerized in the supported V/TiO_2 -AMV catalysts than the supported V/TiO_2 -VTI catalysts.

3.3.2 Steady-state ODH reaction. The steady-state TOF values for propane ODH as a function of surface vanadium density and V-precursor are given in Fig. 11. Reaction conditions correspond to 500 °C with a reactant composition of $\text{C}_3\text{H}_8-\text{O}_2 = 2:1$. Catalyst mass (4–6 mg) or total flow rate (100–180 mL min^{-1}) was varied to find suitable residence times for accurate propane conversion measurements around 10%. The propane ODH TOF values for the AMV precursor modestly increase from 69–132 $\times 10^{-2} \text{ s}^{-1}$ with surface vanadium density up to 8.8 V nm^{-2} . The TOF values for the VTI precursor decrease slightly, from 27.6–15.5 $\times 10^{-2} \text{ s}^{-1}$, with increasing surface vanadium density. The propane ODH TOF values are consistently greater for the supported V/TiO_2 -AMV than V/TiO_2 -VTI catalysts from 3–8.8 V nm^{-2} . The propane ODH TOF values for the two set of catalysts differ by a factor of ~ 2.5 at 3 V nm^{-2} and by a factor of ~ 8.5 at 8.8 V nm^{-2} .

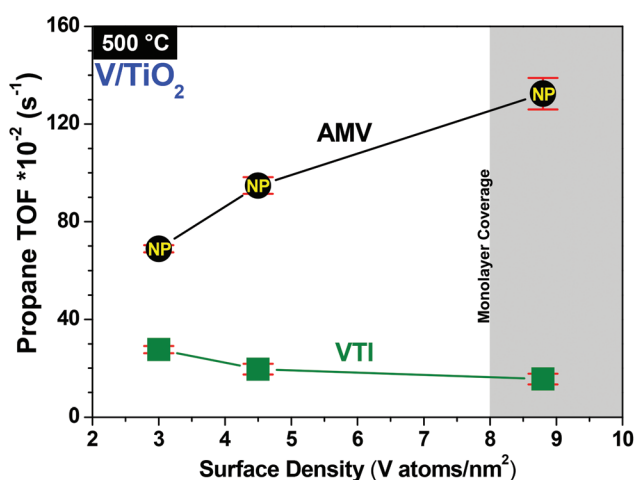


Fig. 11 Steady-state turnover-frequencies (TOFs) for supported V/TiO_2 catalysts during propane oxidative dehydrogenation (ODH) as a function of surface vanadium density and precursor. Reaction conditions correspond to 500 °C with a reactant composition of $\text{C}_3\text{H}_8-\text{O}_2 = 2:1$. Catalyst mass (4–6 mg) or total flow rate (100–180 mL min^{-1}) was varied to find suitable residence times for accurate propane conversion measurements around 10%. “NP” indicates that crystalline V_2O_5 nanoparticles were detected by Raman spectroscopy. Precursors: AMV = ammonium metavanadate/aqueous oxalic acid, VTI = vanadyl triisopropoxide/isopropanol.

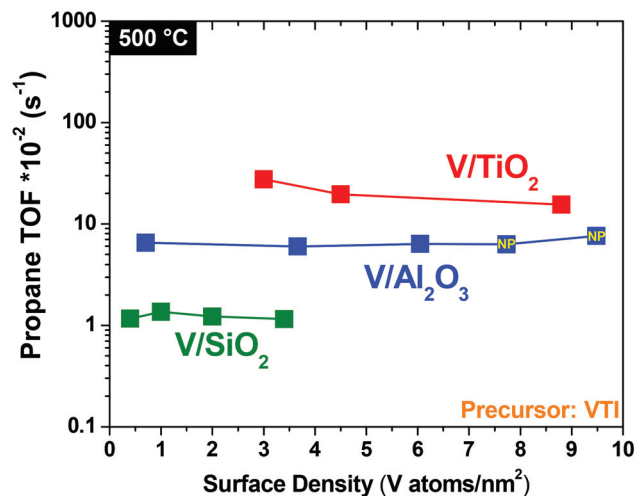


Fig. 12 Steady-state turnover-frequencies (TOFs) for supported $\text{V}/\text{Al}_2\text{O}_3$, V/TiO_2 , and V/SiO_2 catalysts during propane oxidative dehydrogenation (ODH) as a function of surface density. Data shown are only for catalysts prepared using vanadium triisopropoxide (VTI) to demonstrate the effect of oxide support on TOF. “NP” indicates that V_2O_5 nanoparticles were detected by Raman spectroscopy.

3.4 Influence of oxide support on steady-state ODH

The steady-state turnover frequency values for propane ODH as a function of surface vanadium density and oxide support are given in Fig. 12 for the supported vanadia catalysts synthesized with the VTI precursor. The TOF values per surface vanadia site vary by almost two orders of magnitude with the specific oxide support ($\text{TiO}_2 > \text{Al}_2\text{O}_3 > \text{SiO}_2$). These kinetic results demonstrate the significant impact that the oxide support has upon the specific reactivity of the supported vanadium oxide catalytic active sites, as reported many times in the catalysis literature.^{30,35,41,47,48} Qualitatively similar trends were also obtained for propane ODH by the supported vanadia catalysts synthesized with the AMV precursor (not shown for brevity).

4. Discussion

4.1 Influence of vanadium precursor on nature of supported VO_x phases

Below monolayer coverage or maximum dispersion, the vanadium precursor affects the nature of the supported VO_x phase with the trend for formation of crystalline V_2O_5 NPs being $\text{AMV} > \text{VAA} > \text{VTI}$ as reflected in the Raman spectra (see Fig. 1–3, 6, 7, 9, 10). The formation of well-defined and ordered crystalline V_2O_5 NPs also follows the same trend. The crystalline V_2O_5 NP formation trend for the different precursors is also independent of the specific oxide support and only related to the precursor and its impregnation procedure. The order of magnitude greater Raman cross-section for crystalline V_2O_5 NPs than surface VO_4 species indicates that the V_2O_5 NPs are only a minor fraction of the total supported vanadia phase.⁴⁹ This is also reflected in the very similar UV-vis E_g values for the supported VO_x catalysts at the same surface

vanadia density with and without the V_2O_5 NPs (see Fig. 4). By analogy with HR-TEM of supported WO_3/Al_2O_3 catalysts,⁴² the V_2O_5 NPs formed from the VTI precursor are ~ 1 nm and those from the AMV precursor are slightly larger at ~ 2 – 3 nm on the alumina support. The oligomerization of the surface VO_x species with coverage on Al_2O_3 is reflected in the blue shift of the $V=O$ vibration due to vibrational coupling of adjacent vanadyls³⁹ and the decreasing UV-vis optical E_g value with surface vanadia coverage. The slight red shift of the $V=O$ vibrations for the supported VAA catalysts relative to the supported VTI and AMV catalysts suggests that for comparable intermediate surface vanadia coverage the surface vanadia species may be least polymerized with the VAA precursor. In summary, only surface VO_x species are present below $4 V nm^{-2}$ for the supported V/Al_2O_3 catalysts and formation of the surface VO_x species is independent of the specific precursor. This result is related to the strong interaction of the precursors with the alumina support.⁵⁰ Above $4 V nm^{-2}$ for the supported V/Al_2O_3 catalysts, the relative population of crystalline V_2O_5 NPs is strongly dependent on the precursor employed ($AMV > VAA > VTI$). These relative trends also hold for other oxide supports.

For the supported V/SiO_2 and V/TiO_2 catalyst series, the VTI precursor resulted in catalysts with only surface vanadia species while the AMV precursor always resulted in the formation of crystalline V_2O_5 NPs and surface vanadia species.

4.2 Influence of supported VO_x phases on specific propane ODH activity

For the supported V/Al_2O_3 catalysts at low coverage ($< 4 V nm^{-2}$), the propane ODH TOF values are essentially independent of surface vanadium coverage and precursor employed. The independence of the TOF on the relative population of the oligomeric/monomeric surface VO_4 sites indicates that both isolated and oligomeric surface VO_4 species possess the same TOF value for propane ODH. The relatively constant TOF value for the supported V/TiO_2 -VTI catalysts also indicates that the isolated and oligomeric surface VO_4 sites possess the same specific reactivity for propane ODH. For the supported V/SiO_2 catalysts prepared with the VTI precursor, the propane ODH TOF is also constant with surface vanadium density, but this catalyst only contains isolated surface VO_4 sites.³⁰ The specific activity of the surface VO_4 species, monomers and polymers, are only dependent on the specific oxide support, as previously reported by many researchers.^{30,35,41,47,48} This effect can be assigned to the influence of the support material on the reducibility of the surface vanadium oxide sites.⁴⁸

The relative population of the crystalline V_2O_5 /surface VO_4 species for the supported V/Al_2O_3 catalysts with surface vanadium density greater than $4 V nm^{-2}$ is strongly dependent on the precursor employed, as demonstrated by a comparison of Raman band intensities in Table 1. Both the supported V/Al_2O_3 -VTI and V/Al_2O_3 -VAA catalysts only possess trace amounts of V_2O_5 NPs at their highest loading and exhibit constant TOF values for propane ODH as a function surface vanadium density below monolayer coverage ($8 V nm^{-2}$). The

Table 1 Intensity ratios of V_2O_5 - VO_4 Raman bands ($1000 : 1035 cm^{-1}$) for V/Al_2O_3 catalysts

| V/nm^{-2} | AMV precursor | VTI precursor |
|-------------|---------------|---------------|
| 6.1 | 1.6 | — |
| 7.7 | 2.7 | 0.8 |
| 9.5 | 2.9 | 1.1 |

constant propane ODH TOF reflects the comparable TOF values for isolated and oligomeric surface VO_4 species. The slightly higher TOF values for the supported V/Al_2O_3 -VTI and V/Al_2O_3 -VAA catalysts at the highest surface vanadium density reflect the trace of V_2O_5 NPs. The propane ODH TOF value for the supported V/Al_2O_3 -AMV, however, exhibits a strong bell-shaped dependence on the surface vanadium density. The initial increase in TOF coincides with the appearance of crystalline V_2O_5 NPs and the subsequent decrease in TOF coincides with the formation of larger V_2O_5 NPs, especially above monolayer coverage. This reactivity trend surprisingly reveals that very small V_2O_5 NPs exhibit enhanced specific reactivity for the propane ODH reaction. The higher activity of supported V/SiO_2 and V/TiO_2 catalysts containing V_2O_5 NPs compared to the same supported catalysts without V_2O_5 NPs further supports this new conclusion that V_2O_5 NPs in the 1–3 nm range possess enhanced reactivity for propane ODH (see Fig. 8 and 11). In addition to the increased TOF the apparent activation energy is decreased in this range of vanadia surface densities.²⁹

4.3 Origin of the conflicting reactivity trends reported in the catalysis literature

A careful examination of the literature for propane ODH by supported vanadia catalysts reveals that the different reported reactivity trends are directly due to the use of different V-precursors in these studies. Those studies that employed V-precursors/synthesis methods that do not form V_2O_5 NPs in the sub-monolayer region, reported no dependence of the propane ODH TOF on the surface vanadium density below monolayer coverage, as reported in this work.^{19,21,23,25–32} Researchers that employed V-precursors/synthesis methods that form V_2O_5 NPs in the sub-monolayer region, reported that the propane ODH TOF was dependent on the surface vanadium density.^{8,16–18,20,22,24} The present study demonstrates that the choice of V-precursor/synthesis method can lead to the formation of small, highly reactive V_2O_5 NPs (~ 1 – 3 nm) in the sub-monolayer coverage region whose presence is responsible for the conflicting reactivity trends reported for propane ODH by supported vanadia catalysts. This new conclusion stresses the importance of careful and systematic catalyst characterization when comparing reactivity trends in the open literature.

5. Conclusions

Three different precursors (2-propanol/vanadyl triisopropoxide [$VO(O-Pri)_3$] (VTI), oxalic acid/ammonium metavanadate

[NH₄VO₃] (AMV), and toluene/vanadyl acetylacetonate [VO(C₅H₇O₂)₂] (VAA) were used to synthesize supported vanadium oxide catalysts on Al₂O₃, SiO₂, and TiO₂ supports. *In situ* Raman spectroscopy revealed that the choice of the vanadium precursor does not affect the dispersion of the supported vanadium oxide phase below 4 V nm⁻² (~0.5 monolayer coverage) for these syntheses, where only isolated and oligomeric surface VO₄ species are present. Above 4 V nm⁻² (>0.5 monolayer coverage), the relative population of crystalline V₂O₅ NPs is strongly dependent on the precursor employed (AMV > VAA > VTI) with AMV favoring the formation of NPs below monolayer coverage (8 V nm⁻²).

The propane ODH specific reactivity trend demonstrates that there is no significant difference in TOF for the isolated and oligomeric surface VO₄ sites. Surprisingly, crystalline V₂O₅ NPs in the ~1–2 nm range exhibit anomalously high propane ODH TOF values. This comparative study with different V-precurors and synthesis methods finally resolves the debate in the catalysis literature about the dependence of TOF on the vanadium surface density and demonstrates that the greater TOF occasionally assigned to polymeric surface vanadia sites at higher coverage is actually related to the presence of crystalline V₂O₅ NPs below monolayer coverage with enhanced catalytic activity.

Acknowledgements

R.S. and C.A.C. gratefully acknowledge support by the German Research Foundation (Deutsche Forschungsgemeinschaft, DFG) through the cooperative research center “Structure, dynamics, and reactivity of transition metal oxide aggregates” (Sonderforschungsbereich 546, <http://www.chemie.hu-berlin.de/sfb546>). I.E.W. and C.J.K. gratefully acknowledge support provided by the National Science Foundation (Grant CBET-1134012).

Notes and references

- 1 E. Derouane, V. Parmon, F. Lemons and F. Ribeiro, in *NATO Science Series. Mathematics, Physics and Chemistry*, Springer, 2003, vol. 191, p. 218.
- 2 H. Kung, *Adv. Catal.*, 1994, **40**, 1–38.
- 3 E. Mamedov and V. Cortes Corberan, *Appl. Catal., A*, 1995, **127**, 1–40.
- 4 S. Albonetti, F. Cavani and F. Trifiro, *Catal. Rev. Sci. Eng.*, 1996, **38**, 413–438.
- 5 I. E. Wachs and B. M. Weckhuysen, *Appl. Catal., A*, 1997, **157**, 67–90.
- 6 T. Blasco and J. Lopez Nieto, *Appl. Catal., A*, 1997, **157**, 117–142.
- 7 M. A. Bañares, *Catal. Today*, 1999, **51**, 319–348.
- 8 A. Khodakov, B. Olthof, A. T. Bell and E. Iglesia, *J. Catal.*, 1999, **181**, 205–216.
- 9 K. Chen, A. Khodakov, J. Yang, A. T. Bell and E. Iglesia, *J. Catal.*, 1999, **186**, 325–333.
- 10 K. Chen, S. Xie, E. Iglesia and A. T. Bell, *J. Catal.*, 2000, **189**, 421–430.
- 11 K. Chen, E. Iglesia and A. T. Bell, *J. Phys. Chem. B*, 2001, **105**, 646–653.
- 12 E. V. Kondratenko and M. Baerns, *Appl. Catal., A*, 2001, **222**, 133–143.
- 13 I. E. Wachs, *Appl. Catal., A*, 2011, **391**, 36–42.
- 14 I. E. Wachs and C. A. Roberts, *Chem. Soc. Rev.*, 2010, **39**, 5002–5017.
- 15 X. Gao and I. E. Wachs, *J. Phys. Chem. B*, 2000, **104**, 1261–1268.
- 16 K. Chen, A. T. Bell and E. Iglesia, *J. Catal.*, 2002, **209**, 35–42.
- 17 Y. Liu, Y. Cao, K. Zhu, S. Yan, W. Dai, H. He and K. Fan, *Chem. Commun.*, 2002, 2832–2833.
- 18 Y. Liu, Y. Cao, S. Yan, W. Dai and K. Fan, *Catal. Lett.*, 2003, **88**, 61–67.
- 19 Y. Liu, Y. Cao, N. Yi, W. Feng, W. Dai, S. Yan, H. He and K. Fan, *J. Catal.*, 2004, **224**, 417–428.
- 20 S. Yang, E. Iglesia and A. T. Bell, *J. Phys. Chem. B*, 2005, **109**, 8987–9000.
- 21 E. V. Kondratenko, M. Cherian and M. Baerns, *Catal. Today*, 2006, **112**, 60–63.
- 22 O. Schwarz, D. Habel, O. Ovsitser, E. V. Kondratenko, C. Hess, R. Schomäcker and H. Schubert, *J. Mol. Catal. A: Chem.*, 2008, **293**, 45–52.
- 23 S. A. Karakoulia, K. S. Triantafyllidis, G. Tsilomelekis, S. Boghosian and A. Lemonidou, *Catal. Today*, 2009, **141**, 245–253.
- 24 B. Schimmoeller, Y. Jiang, S. E. Pratsinis and A. Baiker, *J. Catal.*, 2010, **274**, 64–75.
- 25 B. Solsona, T. Blasco, J. M. Lopez Nieto, M. L. Pena, F. Rey and A. Vidal-Moya, *J. Catal.*, 2001, **203**, 443–452.
- 26 A. Christodoulakis, M. Machli, A. Lemonidou and S. Boghosian, *J. Catal.*, 2004, **222**, 293–306.
- 27 E. V. Kondratenko, M. Cherian, M. Baerns, D. Su, R. W. X. Schlogl and I. E. Wachs, *J. Catal.*, 2005, **234**, 131–142.
- 28 Y. Liu, W. Feng, T. Li, H. He, W. Dai, W. Huang, Y. Cao and K. Fan, *J. Catal.*, 2006, **239**, 125–136.
- 29 D. Shee, T. Rao and G. Deo, *Catal. Today*, 2006, **118**, 288–297.
- 30 H. Tian, E. I. Ross and I. E. Wachs, *J. Phys. Chem. B*, 2006, **110**, 9593–9600.
- 31 O. Ovsitser, M. Cherian and E. V. Kondratenko, *J. Phys. Chem. C*, 2007, **111**, 8594–8602.
- 32 P. Gruene, T. Wolfram, K. Pelzer, R. Schlogl and A. Trunschke, *Catal. Today*, 2010, **157**, 137–142.
- 33 M. D. Argyle, K. Chen, A. T. Bell and E. Iglesia, *J. Catal.*, 2002, **208**, 139–149.
- 34 B. Frank, A. Dinse, O. Ovsitser, E. V. Kondratenko and R. Schomäcker, *Appl. Catal., A*, 2007, **323**, 66–76.
- 35 A. Dinse, B. Frank, C. Hess, D. Habel and R. Schomäcker, *J. Mol. Catal. A: Chem.*, 2008, **289**, 28–37.

- 36 G. T. Went, S. T. Oyama and A. T. Bell, *J. Phys. Chem.*, 1990, **94**, 4240–4246.
- 37 M. A. Vuurman and I. E. Wachs, *J. Phys. Chem.*, 1992, **96**, 5008–5016.
- 38 B. Olthof, A. Khodakov, A. T. Bell and E. Iglesia, *J. Phys. Chem. B*, 2000, **104**, 1516–1528.
- 39 M. Barton, H. Abbot, O. Bondarchuk, D. Stacchiola, A. Uhl, S. Shaikhutdinov, H. Freund, C. Popa, M. V. Ganduglia-Pirovano, J. Sauer and J. Sauer, *Angew. Chem., Int. Ed.*, 2009, **48**, 8006–8009.
- 40 N. Das, H. Eckert, H. Hu, I. E. Wachs, J. F. Walzer and F. J. Feher, *J. Phys. Chem.*, 1993, **97**, 8240–8243.
- 41 G. Deo and I. E. Wachs, *J. Catal.*, 1994, **146**, 323–334.
- 42 T. Kim, A. Burrows, C. J. Kiely and I. E. Wachs, *J. Catal.*, 2007, **246**, 370–381.
- 43 I. E. Wachs, *Catal. Today*, 1996, **27**, 437–455.
- 44 X. Gao, S. R. Bare, B. M. Weckhuysen and I. E. Wachs, *J. Phys. Chem. B*, 1998, **102**, 10842–10852.
- 45 P. McMillan, *Am. Mineral.*, 1984, **69**, 622–644.
- 46 G. Deo, A. M. Turek, I. E. Wachs, T. Machej, J. Haber, N. Das, H. Eckert and A. Hirt, *Appl. Catal., A*, 1992, **91**, 27–42.
- 47 G. Deo and I. E. Wachs, *J. Catal.*, 1991, **129**, 307–312.
- 48 B. Beck, M. Harth, N. G. Hamilton, C. Carrero, J. J. Uhlrich, A. Trunschke, S. Shaikhutdinov, H. Schubert, H. Freund, R. Schlogl, J. Sauer and R. Schomacker, *J. Catal.*, 2012, **296**, 120–131.
- 49 S. Xie, E. Iglesia and A. T. Bell, *Langmuir*, 2000, **16**, 7162–7167.
- 50 H. Knozinger and E. Taglauer, *Catalysis*, 1993, **10**, 1–40.